Hue University Journal of Science: Natural Science
Vol. 134, No. 1D, 33–47, 2025

pISSN 1859-1388
eISSN 2615-9678

Green-synthesised $NiFe_2O_4$-CQDs composite for sensitive electrochemical detection of acetaminophen and caffeine

Vo Chau Ngoc Anh[1]*, Do Mai Nguyen[2], Nguyen Quang Man[1], Pham Thi Huyen Thoa[3], Tran Ngoc Tuyen[2]

[1] University of Medicine and Pharmacy, Hue University, 530000, Vietnam
[2] University of Sciences, Hue University, 530000, Vietnam
[3] Department of Natural Sciences & Technology, Tay Nguyen University, 630000, Vietnam

* Correspondence to Vo Chau Ngoc Anh <vcnanh@hueuni.edu.vn>

(*Received: 27 August 2025; Revised: 08 October 2025; Accepted: 05 November 2025*)

Abstract. In this study, a $NiFe_2O_4$-CQDs composite was synthesised and utilised to modify a glassy carbon electrode (GCE) for the simultaneous electrochemical detection of acetaminophen (ACP) and caffeine (CFE). The composite material was characterised with various techniques, including FTIR and PL spectroscopy, which confirmed its suitability for electrochemical applications. The DP-ASV method was employed to determine the limit of detection for ACP and CFE, which were found to be 0.35 μM and 0.34 μM, respectively. The electrochemical method exhibited a wide linear range from 0.5 to 11.9 μM for both analytes. Optimised experimental conditions, namely accumulation potential, accumulation time, and pulse amplitude, contributed to high sensitivity, reproducibility, and accuracy in detecting the investigated compounds. Recovery studies in pharmaceutical samples demonstrated reliable results, with recoveries ranging from 94.2 to 103.2%. These findings suggest that the NIF-CQDs-modified GCE is a promising candidate for rapid and accurate electrochemical analysis of ACP and CFE in real-world applications.

Keywords: $NiFe_2O_4$-CQDs composite, electrochemical sensing, acetaminophen, caffeine, differential pulse- anodic stripping voltammetry

1 Introduction

The widespread consumption of pharmaceutical products has led to their increasing presence in various environmental and biological matrices. Among them, acetaminophen (ACP) and caffeine (CFE) are of particular interest because of their extensive global use, both individually and in co-formulated products designed to enhance analgesic efficacy [1–3]. Their frequent co-occurrence, for instance, in combination drug tablets and urban wastewater effluents, necessitates the development of analytical methods capable of their reliable and simultaneous quantification. This capability is crucial for applications such as pharmaceutical quality assurance, clinical diagnostics, and environmental risk assessment [4–6].

To address this analytical demand, established instrumental methods, such as liquid chromatography [7] and mass spectrometry [8], have been extensively applied, offering high selectivity and precision. However, these techniques, although robust, are often limited by constraints. These include significant capital investment for instrumentation, complex sample preparation protocols, and substantial operational time, which can impede their deployment for rapid or high-throughput screening purposes [9, 10]. Such constraints have motivated the continued exploration of alternative analytical

platforms that offer a more favourable balance of performance, cost, and operational simplicity [11, 12].

In this regard, electrochemical sensing platforms have emerged as a promising alternative for determining electroactive pharmaceutical compounds [13]. These methods are distinguished by a suite of advantageous features, including high intrinsic sensitivity, rapid response times, low-cost instrumentation, and amenability to miniaturisation for portable, on-site applications [14–16]. Despite these merits, the direct electroanalysis of ACP and CFE at unmodified electrodes is often hindered by slow electron transfer kinetics and the significant overlap of their voltammetric signals, originating from their similar oxidation potentials [1, 17]. It is widely recognised that the functionalisation of the electrode surface with carefully designed materials is an effective strategy to surmount these challenges by facilitating charge transfer and improving peak resolution [18, 19].

The targeted enhancement of electrode performance is frequently achieved through the rational design of nanocomposite materials that leverage synergistic effects of the constituent components. Within this framework, spinel ferrites, such as nickel ferrite ($NiFe_2O_4$), have been investigated as promising electrocatalytic modifiers because of their favourable electronic properties, high chemical stability, and inherent catalytic activity [20, 21]. To further augment performance, these metal oxides are often integrated with conductive carbonaceous supports. Carbon quantum dots (CQDs) are particularly well-suited for this role, possessing excellent electrical conductivity, a high surface-to-volume ratio, and versatile surface chemistry that can promote analyte interaction and charge transfer [22]. It is hypothesised that the formation of a $NiFe_2O_4$-CQDs composite could yield a material where the CQDs network provides a highly conductive pathway and prevents the aggregation of $NiFe_2O_4$ particles, thereby maximising the exposure of their catalytically active sites [23].

Further refining this material's design approach, considerable research effort is now being directed towards sustainable synthesis protocols that adhere to the principles of green chemistry. The synthesis of CQDs from low-cost, renewable, and non-toxic biomass precursors is a key example of this trend [24, 25]. The utilisation of abundant biopolymers, such as starch, presents an especially attractive route, offering an environmentally benign alternative to conventional synthetic methods [26, 27]. Accordingly, the present work is focused on the synthesis and characterisation of a $NiFe_2O_4$-CQDs composite, wherein the CQDs are derived from starch. This material was subsequently employed to modify a glassy carbon electrode (GCE), and its efficacy as a sensor for the simultaneous voltammetric determination of ACP and CFE was systematically evaluated by means of differential pulse voltammetry.

2 Experimental

2.1 Chemicals

The chemicals used in this study include nickel nitrate ($Ni(NO_3)_2{\cdot}6H_2O$), iron nitrate ($Fe(NO_3)_3{\cdot}9H_2O$), starch, magnesium chloride ($MgCl_2$), calcium hydrogen phosphate ($Ca(HPO_4)_2$), zinc chloride ($ZnCl_2$), sodium sulfate (Na_2SO_4), aluminum nitrate ($Al(NO_3)_3$), ascorbic acid, sodium benzoate, and D-glucose. These reagents were purchased from Merck, Germany, and Xilong, China. All chemicals were of analytical grade and used without further purification, ensuring their suitability for electrochemical analysis.

pISSN 1859-1388
eISSN 2615-9678

2.2 Instruments

The Fourier-transform infrared (FT-IR) spectra, recorded in the range of 4000–400 cm^{-1}, were obtained with an IR-Prestige-21 spectrometer (Shimadzu, Japan). Additionally, photoluminescence (PL) spectra were collected with the Fluorolog 3 FL3-22 fluorometer from Horiba.

Electrochemical investigations were performed with the CPA-HH5 computerised polarography analyser, designed and produced in Vietnam. In these experiments, a conventional three-electrode setup was employed, comprising an Ag/AgCl electrode saturated with 3.0 M KCl as the reference electrode, a platinum wire serving as the auxiliary electrode, and a bare glassy carbon electrode with a diameter of 2.8 mm as the working electrode.

2.3 Synthesis of $NiFe_2O_4$, CQDs and $NiFe_2O_4$-CQDs

$NiFe_2O_4$-CQDs nanocomposites were synthesised from $Ni(NO_3)_2{\cdot}6H_2O$, $Fe(NO_3)_3{\cdot}9H_2O$, and starch $(C_6H_{10}O_5)_n$ as precursors via a hydrothermal method. The reagents were mixed at an $n_{Ni}/n_{Fe}/n_{starch}/n_{H_2O}$ molar ratio of 2:1:4.5:540 (acceptable to use a mole of starch monomeric units), dissolved in deionised (DI) water, and heated to 80–85 °C for 1 h to ensure starch's complete dissolution. The resulting solution was transferred into a 100 mL Teflon-lined stainless steel autoclave and maintained at 180 °C for 24 h. The obtained brown precipitate was centrifuged, thoroughly washed with DI water several times, and dried at 100 °C for 24 h, yielding the composite material, denoted as NIF-CQDs. Pure $NiFe_2O_4$ nanoparticles, denoted as NIF, were obtained by calcining the as-prepared NIF-CQDs at 700 °C for 3 h, which effectively removed the carbon quantum dots. For comparison, CQDs were synthesised under the same hydrothermal conditions at 180 °C for 24 h but in the absence of nickel and iron salts. The product was subsequently evaporated at 100 °C for 48 h and dried to obtain pure CQDs [28–30].

2.4 Modification of GCE with $NiFe_2O_4$, CQDs and $NiFe_2O_4$-CQDs

A glassy carbon electrode (diameter 2.8 ± 0.1 mm) was first polished with alumina slurry of 0.05 μm particle size, followed by thorough rinsing with 1 M HNO_3, absolute ethanol, and DI water to remove residual alumina particles. Suspensions of the modifiers were prepared by dispersing 5 mg of NIF, CQDs, or NIF-CQDs in 5 mL of DI water, followed by ultrasonic treatment for 5 h to obtain stable dispersions (1 mg/mL). The electrode modification was carried out by drop-casting 5 μL of each suspension onto the clean GCE surface, which was then dried naturally at ambient temperature to obtain the NIF/GCE, CQDs/GCE, and NIF-CQDs/GCE electrodes, respectively.

2.5 Preparation of practical samples

Weigh accurately 10 dosage units (tablets/capsules) and calculate the average weight of the 10 units. Grind the samples into fine powder in a mortar, then weigh an appropriate amount of powder (equivalent to 1 tablet for Samples 1 and 2; 2 tablets for Sample 3). Transfer the ground powder into a 100 mL volumetric flask, add 50 mL of water, dissolve, and sonicate for approximately 30 minutes. After cooling, add water up to the mark, shake well, and filter through filter paper (Solution 1). Dilute Solution 1 20 times with water to obtain Solution 2. Then, pipette an accurate volume of Solution 2 into an electrochemical cell, add 10 mL of Britton-Robinson buffer solution (BRBS, 0.02 M, pH 8.0), and perform DP-ASV analysis to determine the ACP/CFE content in each sample using previously optimised DP-ASV parameters.

For recovery experiments, the same procedure was repeated, but prior to analysis, known amounts of ACP and CFE standard solutions were spiked into Solution 2 (noted as spiked samples). The recovery percentage was calculated according to:

$$\text{Recovery}(\%) = \frac{\text{Measured concentration} - \text{Original concentration}}{\text{Added concentration}} \times 100$$

– **Measured concentration:** This refers to the total concentration of the analyte determined in a real sample after a known amount of standard has been added. It represents the combined concentration from the original sample and the spiked standard.

– **Original concentration:** This is the concentration of the analyte naturally present in the real sample before spiking. In some cases, particularly with trace analysis, this value may be negligible.

– **Added concentration:** This is the accurate, known concentration of the analyte standard that was spiked into the original sample. This value serves as the reference against which the method's efficiency is evaluated.

Table 1. Origin and characteristics of the pharmaceutical samples (*MNG: manufacturing code; EXP: expiration date*)

No	Name	Labeled ACP (mg)	Labeled CFE (mg)	MNG	EXP	Average mass per tablet (g)
1	Hapacol Extra	500	65	30125	40128	0.71
2	Panadol Extra	500	65	30125	0128	0.68
3	Ibuparavic	300	25	EVH2461	11027	0.55

3 Results and discussion

3.1 Characterisation of materials

In Fig. 1, the CQDs show the typical broad O–H/N–H stretching band at ~3400 cm^{-1} and carbon-framework vibrations in the 1650–1500 cm^{-1} region (C=C/C=O and N–H bending), together with C–O/C–O–C stretches around 1200–1000 cm^{-1}. In the $NiFe_2O_4$ reference [31], two strong spinel metal-oxygen modes appear at ~580 and ~430 cm^{-1}, which are attributed to the intrinsic stretching vibrations of Fe–O and Ni–O bonds in the spinel lattice. In the NIF-CQDs composite, the CQDs bands are retained while the ferrite M–O bands emerge in the low-wavenumber region, with slight intensity changes/shifts, indicating the coexistence of CQDs surface functionalities and NIF and suggesting interfacial coupling between the two components. These features confirm the successful formation of the NIF-CQDs hybrid, which is suitable for electrochemical applications [21, 32].

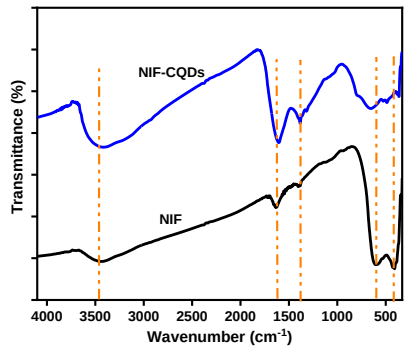

Fig. 1. FTIR of NIF and NIF-CQDs

In Fig. 2, pristine CQDs emit strongly (peak in the green region), whereas NIF-CQDs exhibit marked fluorescence quenching [25, 33]. Such quenching is consistent with electronic coupling between CQDs and NIF (e.g., photo-induced charge/energy transfer and possible inner-filter effects), which typically accompanies faster interfacial electron exchange at electrodes [21]. Accordingly, NIF-CQDs are selected for the subsequent GCE surface modification and electrochemical determination of organic targets.

pISSN 1859-1388
eISSN 2615-9678

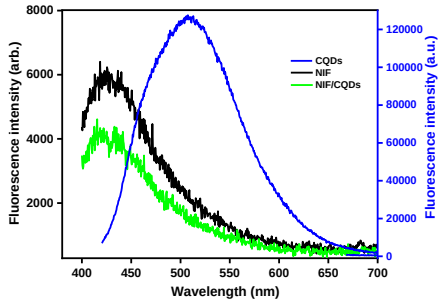

Fig. 2. Fluorescence spectra of CQDs, NIF, and NIF-CQDs
The green and black curves correspond to the left y-axis, while the blue curve corresponds to the right y-axis.

3.2 Simultaneous electrochemical detection of acetaminophen and caffeine by NIF-CQDs/GCE

Electrode behaviour

In Fig. 3a, cyclic voltammograms (CVs) of ACP and CFE recorded at different electrodes reveal a clear ranking of activity. The bare GCE creates the smallest and broadest oxidation waves, consistent with its limited active area and sluggish charge transfer. Introducing CQDs modestly increases the peak currents, indicating better conductivity and more adsorption sites, whereas NIF alone yields a somewhat larger response than CQDs but remains below that of the composites. A pronounced enhancement is obtained with the NIF-CQDs composites that produce the sharpest, highest anodic peaks for both analytes.

These trends are quantified in Fig. 3b: the bar chart of peak currents confirms that NIF-CQDs yields the largest responses for both ACP and CFE, followed by NIF, CQDs, and GCE. The superiority of NIF-CQDs is consistent with two material attributes established earlier: (i) FT-IR features evidencing oxygen-containing surface groups on CQDs and metal-oxygen vibrations of $NiFe_2O_4$ that favour adsorption and interfacial coupling; and (ii) fluorescence quenching of CQDs after coupling with NIF, which points to more efficient photo/charge separation and, by analogy, faster interfacial electron transfer during electro-oxidation. Together, these characteristics rationalise the CV gains: mixed-valence redox centres in $NiFe_2O_4$ (Ni^{2+}/Ni^{3+}, Fe^{2+}/Fe^{3+}) act as catalytic mediators, while CQDs provide a conductive, defect-rich network [34]. On this electrochemical and spectroscopic basis, NIF-CQDs are selected as a suitable modifier for subsequent GCE surface modification and electroanalytical studies on organic analytes.

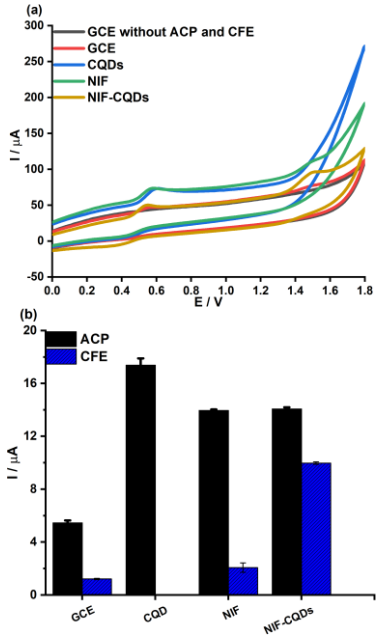

Fig. 3. (a) CVs of ACP and CFE at different electrodes; (b) Peak currents of various electrodes
Experimental conditions: scan rate 20 mV/s; $C_{ACP} = C_{CFE} = 12$ μM in BRBS 0.02 M (pH 5)

Effect of pH

Fig. 4a demonstrates the influence of pH on electrochemical responses. The solution pH significantly affects the electrochemical signals, indicating that the electrooxidation reaction is considerably dependent on proton concentration. As the pH increases, the peak potential shifts linearly. The corresponding regression equations are provided below:

$E_{p,ACP} = (0.999 \pm 0.052) + (-0.065 \pm 0.007) \times pH$; $R^2 = 0.964$ (1)

$E_{p,CFE}$ = (1.821 ± 0.033) + (−0.041 ± 0.005) × pH; R^2 = 0.963 (2)

With the assistance of the Nernst equation, at 298 K (25 °C), the relationship between E_p and pH of a pair of redox and conjugate could be illustrated as follows:

$$E_p = E^0 + \frac{0.059}{n}\log\frac{Ox}{R} - 0.059\frac{m}{n}pH \quad (3)$$

In Equation (3), n denotes the number of electrons transferred and m the number of protons involved in the proton-coupled redox process.

The slope of the E_p versus pH graph was –0.065 for ACP and –0.041 for CFE (Eq. 3), which is close to the Nernstian value of –0.059 (Fig. 4c). This value corresponds to $m/n \approx 1$, indicating that the oxidation of ACP and CFE on the modified electrode involves an equal transfer of electrons and protons. As shown in Fig. 4b, the peak current decreases with the pH, suggesting effective electrochemical detection. In addition, in Fig. 4b, the peak-current plot indicates that both analytes achieve their highest and most reproducible currents at pH 8. At pH 9, a slight current decrease appears, which is reasonable for proton-coupled oxidations when proton availability becomes limited, and the interfacial charge of the film/solution changes.

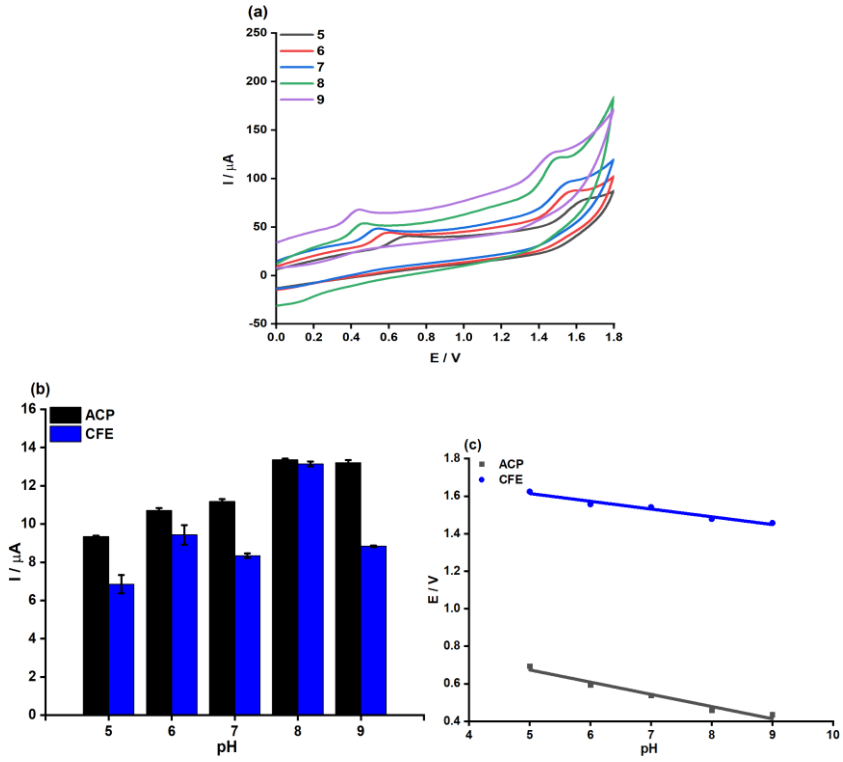

Fig. 4. (a) CVs of ACP and CFE at pH values from 5 to 9; (b) Plot of pH vs. I_p; (c) Plot of pH vs. E_p
Experimental condition: a potential scan range: 0–1.8 V; scan rate: 20 mV/s; in the solution 0.02 M BRBS; $C_{ACP} = C_{CFE} = 12$ *µM*

Effect of accumulation potentials

In Fig. 5, the DP-ASV curves were recorded while the accumulation potential (E_{acc}) varied from 0.0 to +1.0 V (pH 8.0, accumulation 5 s). In Fig. 5a, the peak positions of ACP and CFE remain essentially unchanged, whereas the peak currents depend on E_{acc}. In Fig. 5b, a modest increase in current is observed when a small positive bias is applied, with an E_{acc} of 0.2 V, giving the highest and most reproducible currents for both analytes. At higher biases (≥0.4 V), the currents level off or decrease

pISSN 1859-1388
eISSN 2615-9678

slightly, and no further gain is perceived. On this basis and considering current magnitude, repeatability, and baseline stability, we selected the E_{acc} of 0.2 V as the optimal accumulation potential for the subsequent measurements of ACP and CFE.

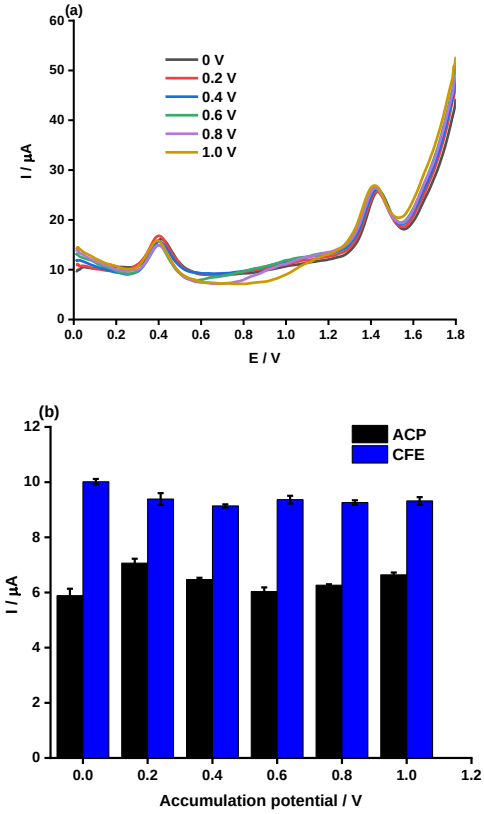

Fig. 5. (a) DP-ASVs of ACP and CFE at different accumulation potentials; (b) Plot of E_{acc} vs. I_p
Experimental conditions: potential scan range of 0–1.0 V; accumulation time 5 s; pulse amplitude: 0.05 V; potential step: 0.005 V; $C_{ACP} = C_{CFE} = 12$ µM in BRBS 0.02 M (pH 8.0)

Effect of accumulation time

The effect of accumulation time (t_{acc}) on ACP and CFE was examined by means of DP-ASV. In Fig. 6a, the peak currents for both analytes increase with accumulation time up to 5 seconds, after which no significant change is observed. Fig. 6b confirms that 5 s gives nearly the same peak current as 10–20 seconds. Therefore, to optimise measurement time without sacrificing sensitivity, we chose the t_{acc} of 5 s for further experiments.

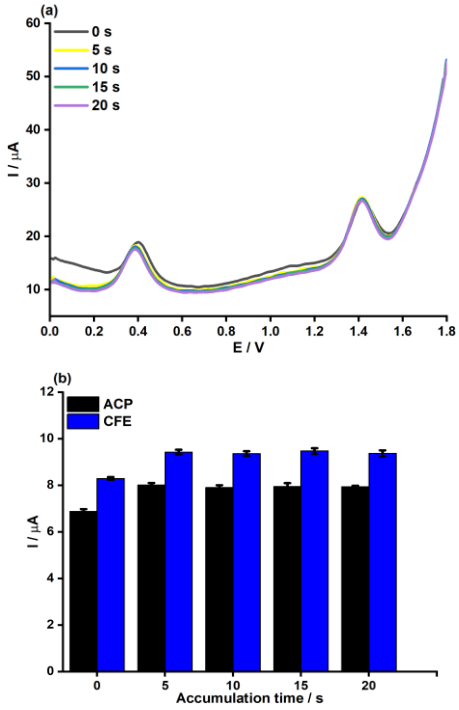

Fig. 6. (a) DP-ASVs of ACP and CFE at different accumulation times, (b) Plot of t_{acc} vs. I_p
Experimental conditions: potential scan range of 0–1.0 V; accumulation potential 0.2 V; pulse amplitude: 0.05 V; potential step: 0.005 V; $C_{ACP} = C_{CFE} = 12$ µM in BRBS 0.02 M (pH 8.0)

Effect of pulse amplitudes

The effect of pulse amplitude (ΔE) on the peak current of ACP and CFE was evaluated by using DP-ASV. In Fig. 7a, the peak currents increase as ΔE is raised, and the ΔE of 0.1 V shows the highest and most stable response. Fig. 7b further confirms that the ΔE of 0.1 V yields the best reproducibility for both analytes, while higher amplitudes fail to lead to significant improvement. Thus, the ΔE of 0.1 V is chosen as the optimal pulse amplitude for further measurements.

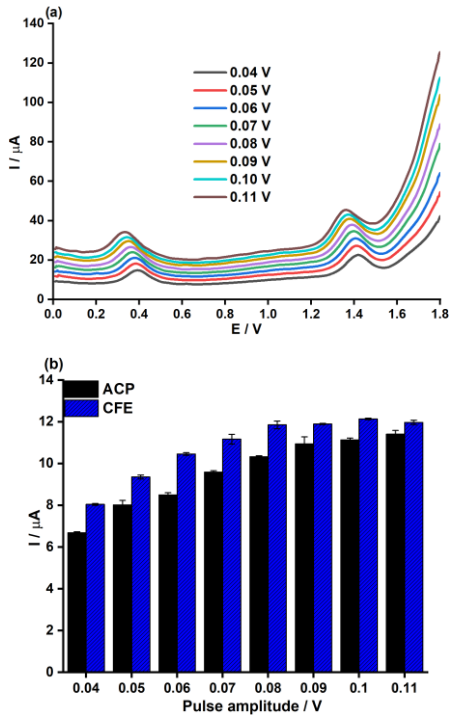

Fig. 7. (a) DP-ASVs of ACP and CFE at different pulse amplitudes; (b) Plot of ΔE vs. I_P
Experimental conditions: potential scan range of 0–1.0 V; accumulation time 5 s; accumulation potential: 0.2 V; potential step: 0.005 V; $C_{ACP} = C_{CFE} = 12$ μM in BRBS 0.02 M (pH 8.0)

Effect of potential steps

The effect of potential steps (U_{step}) on the electrochemical response of ACP and CFE was investigated by using DP-ASV. In Fig. 8a, the peak currents increase slightly as the potential step is increased from 0.004 to 0.009 V, with the currents stabilising at 0.007 V. Fig. 8b confirms that 0.007 V provides the best balance of the peak current and reproducibility, as further increases in the potential step do not significantly enhance the response. Therefore, the U_{step} of 0.007 V is chosen as the optimal value for subsequent experiments.

Table 2 summarises the key parameters and their optimal values for the electrochemical analysis of ACP and CFE. The accumulation potential was set at 0.2 V, providing effective adsorption of the analytes without excessive interference. The 5 s accumulation time was selected, as it yielded optimal peak currents, with no significant improvement observed at longer times. The pulse amplitude was set to 0.1 V, balancing the signal response without introducing unnecessary noise, and the step potential was adjusted to 0.007 V, which provided the optimal current response with stable results. These optimised parameters ensure high sensitivity and reproducibility for the detection of ACP and CFE by the DP-ASV technique.

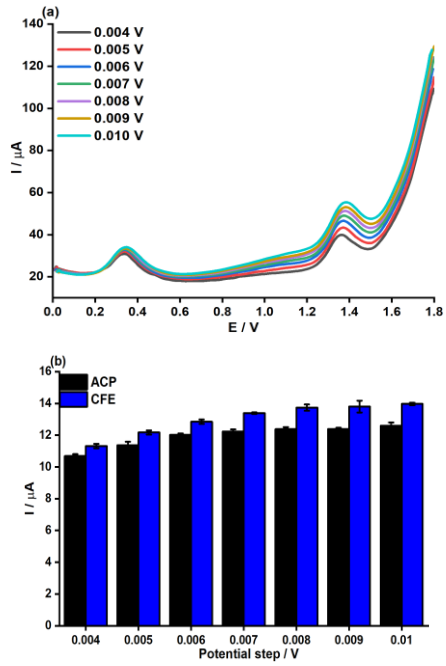

Fig. 8. (a) DP-ASVs of ACP and CFE at different potential steps; (b) Plot of U_{step} vs. I_P
Experimental conditions: potential scan range of 0–1.0 V; accumulation time 5 s; accumulation potential: 0.2 V; pulse amplitude: 0.10 V; $C_{ACP} = C_{CFE} = 12$ μM in BRBS 0.02 M (pH 8.0)

Table 2. Report of several selected parameters

Parameters	Symbol	Value	Unit
Accumulation potential	E_{acc}	0.2	V
Accumulation time	t_{acc}	5	s
Pulse amplitude	ΔE	0.1	V
Step potentials	U_{step}	0.007	V

pISSN 1859-1388
eISSN 2615-9678

Linear range and limit of detection

The individual detection of ACP and CFE was performed with the DP-ASV technique. The concentration of one analyte increases while the other remains constant in the 0.02 M BRBS buffer at pH 8.0 (Fig. 9). The peak current increases with the concentration of the target analyte, while it remains nearly constant for the other, suggesting that the oxidation reactions occur independently. The peak current increases linearly within the concentration range of 0.5 to 4.9 µM. The corresponding regression equations are as follows:

$I_{p,ACP} = (1.23 \pm 0.08) + (1.18 \pm 0.03) \times C_{ACP}$, µM; $R^2 = 0.99$ (4)

$I_{p,CFE} = (-0.29 \pm 0.05) + (1.22 \pm 0.02) \times C_{CFE}$, µM; $R^2 = 0.99$ (5)

In the concentration range of 0.5 to 4.9 µM, the limit of detection (LOD) calculated (3σ formula) for ACP and CFE is 0.31 and 0.20 µM, and the limit of quantification (LOQ) for ACP and CFE is 0.93 and 0.60 µM.

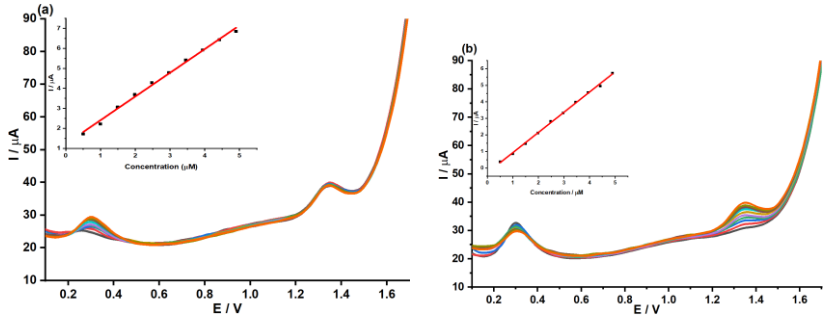

Fig. 9. (a) DP-ASVs of ACP at increasing concentrations (0.5–4.9 µM) with CFE fixed at 4.9 µM; inset: linear plot of I_p vs. C_{ACP}; (b) DP-ASVs of CFE at increasing concentrations (0.5–4.9 µM) with ACP fixed at 4.9 µM; inset: linear plot of I_p vs. C_{CFE}

Experimental conditions: Potential ranges from 0 V to 1.8 V; scan rate: 20 mV/s; pulse amplitude: 0.1 V; accumulation time: 5 s; accumulation potential: 0.2 V

The electrochemical signals for the simultaneous ACP and CFE additions in the 0.02 M BRBS buffer with pH 8.0 at NIF-CQDs/GCE are presented in Fig. 10.

The peak currents of both analytes increase with the increase in ACP and CFE concentration (Fig. 11a). Fig. 11b shows the calibration curves obtained at NIF-CQDs/GCE from various concentrations of ACP and CFE, as follows:

$I_{p,ACP} = (4.503 \pm 0.068) + (0.773 \pm 0.011) \times C_{ACP}$; $R^2 = 0.997$ (7)

$I_{p,CFE} = (-0.052 \pm 0.059) + (1.151 \pm 0.009) \times C_{CFE}$; $R^2 = 0.999$ (8)

The LOD (calculated by using the 3σ method) and LOQ for ACP and CFE were 0.35 µM and 0.34 µM, respectively, for the concentration range. It is noteworthy that the LOD values for ACP and CFE in the simultaneous and individual detection are very similar, suggesting that the oxidation of these compounds at the NIF-CQDs-modified GCE occurs without interference. Thus, simultaneous determination of both ACP and CFE can be successfully achieved without cross-interference. A comparison of the LOD and linear range for ACP and CFE, with values reported in the literature, is provided in Table 3. This table shows that the linear range and LOD of the NIF-CQDs-modified GCE are comparable and even smaller.

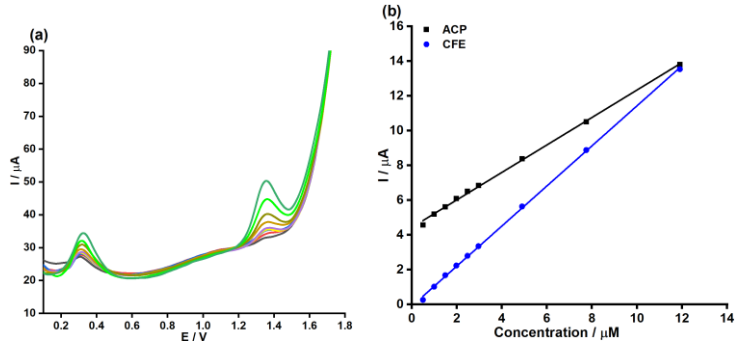

Fig. 10. (a) DP-ASVs of ACP and CFE at increasing concentrations (0.5–11.9 µM); (b) Plot of I_p vs. C_{ACP} and C_{CFE}
Experimental conditions: Potential ranges from 0 V to 1.8 V; scan rate: 20 mV/s; pulse amplitude: 0.1 V; accumulation time: 5 s; accumulation potential: 0.2 V

Table 3. Comparison of the obtained results to other reports

Electrode	Method	Analyte	Linear range (µM)	LOD (µM)
MOF-199/Naf-GCE	DPV	ACP	0.10–5	1.26
		CFE	0.20–5	1.24
Activated-GCE	SWV	ACP	10–180	2.55
		CFE	10–95	2.36
3D-printed sensor	DPV	ACP	0.66–40	2.84
		CFE	0.37–220	2.01
GrRGC	DPV	ACP	0–50	2.01
		CFE		2.31
ErGO/GCE	DP-ASV	ACP	0.2–4.4	0.25
		CFE		0.23
NIF-CQDs/GCE	DP-ASV	ACP	0.5–11.9	0.35
		CFE		0.34

To evaluate the repeatability of the electrochemical detection of ACP and CFE by means of DP-ASV, we performed experiments with the NIF-CQDs-modified GCE at four different concentrations: 2.48, 4.90, 8.45, and 11.9 µM. The peak currents for both ACP and CFE were consistently measured under identical experimental conditions (accumulation potential: 0.2 V; accumulation time: 5 s; pulse amplitude: 0.1 V; step potential: 0.007 V). The values of RSD were calculated for each concentration (n = 10).

From the data presented in Fig. 11, the RSD values for ACP (4, 2.4, 1.3 and 0.9%) and CFE (4.7, 1.5, 1.4 and 0.8%) at all concentrations were well below ½.$RSD_{Horwitz}$ threshold (9.3, 8.4, 7.7 and 7.3% for ACP, and 8.9, 8.1, 7.4 and 7.1% for CFE), indicating good repeatability and reliability of the modified GCE electrode for these analytes. These results demonstrate that the NIF-CQDs-modified GCE electrode exhibits excellent repeatability, making it a reliable tool for the electrochemical determination of ACP and CFE at various concentrations. The RSD values fall well within acceptable limits, confirming the electrode's ability to consistently generate accurate and reproducible results under the given experimental conditions.

pISSN 1859-1388
eISSN 2615-9678

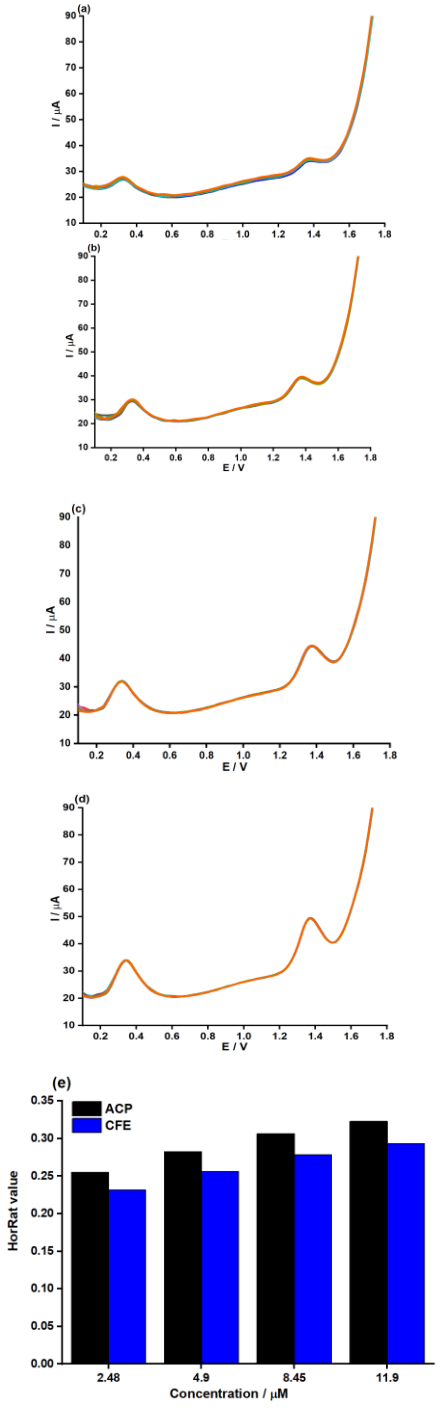

Fig. 11. DP-ASVs of ACP and CFE with different concentrations: (a) 2.48 μM; (b) 4.9 μM; (c) 8.45 μM; (d) 11.9 μM within 0.02 M BRBS buffer (pH 8); (e) HorRat values correspond to the four concentrations (n = 10) *Experimental conditions: potential ranges from 0 V to 1.8 V; scan rate: 20 mV/s; pulse amplitude: 0.1 V; accumulation time: 5 s; accumulation potential: 0.2 V.*

Fig. 12 presents the evaluation of reproducibility and durability for the electrochemical determination of ACP and CFE by using the NIF-CQDs-modified electrode. The peak currents for both ACP and CFE were recorded over seven consecutive measurements with the same experimental procedure. The results show consistent current responses for both analytes, with the RSD values of 4.89% for ACP and 1.89% for CFE. These values indicate excellent reproducibility, confirming that the NIF-CQD modified electrode provides reliable and repeatable performance over multiple cycles.

To assess long-term stability, we used the modified electrode to determine the ACP and CFE concentration over a period of seven days. The peak currents were stable, with the RSD values of 1.19% for ACP and 0.54% for CFE, demonstrating the outstanding durability of the electrode. These results suggest that the electrode maintains its electrochemical performance over extended periods, with a minimal loss in signal intensity, making it a viable option for long-term applications.

Overall, the NIF-CQD modified electrode exhibits both high reproducibility and excellent durability, confirming its suitability for long-term electrochemical sensing applications.

Table 4 illustrates the influence of various interferents on the oxidation peak currents of ACP and CFE, with the relative error (RE%) used to quantify the interference. For ACP, Na_2SO_4 at the molar ratio of 80 caused a slight increase in the peak current with an RE of 4.6%, while $Al(NO_3)_3$ at the 100 molar ratio showed minimal interference with an RE of 1.0%. Other interferents such as $ZnCl_2$ and $Ca(HPO_4)_2$ had moderate effects, with the REs of 3.4% and –3.0%, respectively, while $MgCl_2$ caused a small negative interference with the RE of –2.4%.

For CFE, Na_2SO_4 caused a slight negative shift with the RE of –3.4%, while $Al(NO_3)_3$ produced a more significant negative interference with the RE

of –4.5%. $ZnCl_2$ and $Ca(HPO_4)_2$ had a positive influence, with the REs of 1.4% and 3.3%, respectively, while $MgCl_2$ caused a negative effect with the RE of –1.6%.

For the additional interferents tested, D-glucose and sodium benzoate caused moderate negative effects on both ACP and CFE, with the REs of –3.5% and –4.2% for ACP, and the REs of –4.2% and –4.1% for CFE, respectively. Ascorbic acid had a minor effect on ACP with the RE of 1.9% and a higher impact on CFE with the RE of 4.0%.

Overall, while most interferents cause minimal changes in the peak currents, substances such as Na_2SO_4, $Al(NO_3)_3$, and $Ca(HPO_4)_2$ may lead to significant deviations and should be considered when analysing samples. However, the modified electrode shows a good level of selectivity for ACP and CFE, with the RE values largely falling within acceptable ranges for reliable detection.

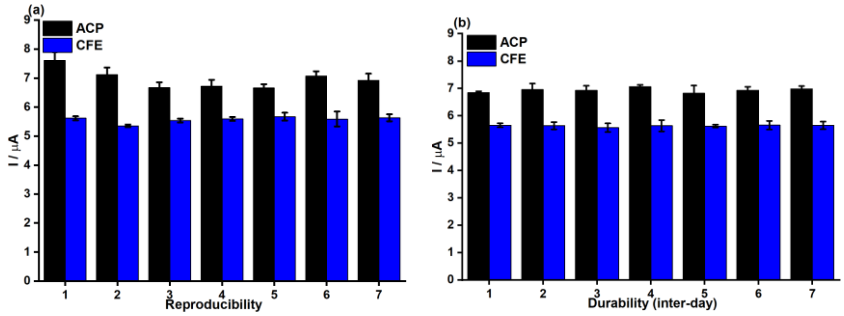

Fig. 12. Peak current I_p for $C_{ACP} = C_{CFE} = 4.90$ μM in 0.02 M BRBS buffer pH 8 (a) on the electrode modified with NIF-CQDs for 7 times with the same procedure; (b) for seven days of durability

Experimental conditions: potential ranges from 0 V to 1.8 V; scan rate: 20 mV/s; pulse amplitude: 0.1 V; accumulation time: 5 s; accumulation potential: 0.2 V.

Table 4. Influence of oxidation peak current interferents (4 μM ACP and 4μM CFE within 0.02 M BRBS solution with pH 8)

Interferents	Interferent - ACP molar ratio	*RE* (%)	Interferent – CFE molar ratio	*RE* (%)
Na_2SO_4	80	4.6	100	-3.4
$Al(NO_3)_3$	100	1.0	100	-4.5
$ZnCl_2$	100	3.4	100	1.4
$MgCl_2$	60	-2.4	100	-1.6
$Ca(HPO_4)_2$	100	-3.0	100	3.3
D-Glucose	100	-3.5	50	-4.2
Sodium benzoate	100	-4.2	50	-4.1
Ascorbic acid	100	1.9	50	4.0

pISSN 1859-1388
eISSN 2615-9678

Analysis of real samples

The DP-ASV method was applied to determine the concentrations of ACP and CFE in pharmaceutical samples, with the recovery values used to assess the accuracy of the method. The recoveries obtained for each sample are shown in Table 5.

For Hapacol Extra, the recovery for ACP was 98.1%, and for CFE, it was 94.2%. These values suggest that the method provides reliable results with minimal deviation from the expected values. For Panadol Extra, the recovery for ACP was 102.4%, and for CFE, it was 103.2%; both of which are within the acceptable range, indicating high accuracy for this formulation. In the case of Ibuprofen, the recovery for ACP was 95.4%, and for CFE, it was 101.2%, demonstrating that the method is also effective for this sample, with recoveries close to the expected values. Overall, the recoveries from all real samples range from 94.2 to 103.2%, confirming that the DP-ASV method is suitable for determining ACP and CFE concentrations in pharmaceutical products with high accuracy.

Table 5. ACP and CFE concentrations determined via DP-ASV in the medicine models

Samples	Analyte	Content ± SD (μM)	Content compared to the label (%)	Spiked (μg)	Found ± SD (μg)	*Rev.* (%)
Hapacol Extra (ACP: 500 mg, CFE: 65)	ACP	512.4 ± 4.1	102.5	1.5	1.5 ± 0.02	98.1
	CFE	64.1 ± 1.1	98.6	1.9	1.8 ± 0.03	94.2
Panadol Extra (ACP: 500 mg, CFE: 65)	ACP	488.5 ± 2.3	97.7	1.5	1.6 ± 0.02	102.4
	CFE	63.1 ± 0.7	96.9	1.9	2.1 ± 0.03	103.2
Ibuparavic (ACP: 300 mg, CFE: 25)	ACP	292.2 ± 5.2	97.4	1.5	1.4 ± 0.02	95.4
	CFE	25.9 ± 0.5	103.9	1.9	1.9 ± 0.03	101.2

4 Conclusion

The $NiFe_2O_4$-CQDs-modified GCE demonstrated high performance for the simultaneous electrochemical determination of acetaminophen and caffeine. The method was optimised for accuracy and reproducibility, with the LOD values of 0.35 μM for acetaminophen and 0.34 μM for caffeine. The wide linear range of 0.5 μM to 11.9 μM was achieved for both analytes. The method showed excellent reproducibility and accuracy, as evidenced by recoveries ranging from 94.16% to 103.24% in real pharmaceutical samples. These results confirm the potential of the $NiFe_2O_4$-CQDs-modified GCE for accurate, sensitive, and reliable electrochemical sensing of acetaminophen and caffeine. This approach offers an efficient and eco-friendly alternative for routine analysis in pharmaceutical and clinical applications.

Acknowledgement

This research was funded by the University of Medicine and Pharmacy, Hue University, under grant number 10/25.

Conflict of Interest

The authors declare that there are no conflicts of interest regarding the publication of this paper.

References

1. Habibi B, Jahanbakhshi M, Abazari M. A modified single-walled carbon nanotubes/carbon-ceramic electrode for simultaneous voltammetric determination of paracetamol and caffeine. Journal of the Iranian Chemical Society. 2014;11(2):511-21.
2. Demir N, Atacan K, Ozmen M, Bas SZ. Design of a new electrochemical sensing system based on MoS_2-TiO_2/reduced graphene oxide nanocomposite for the detection of paracetamol. New J Chem. 2020;44:11759-67.
3. Švorc Ľ, Strežová I, Kianičková K, Stanković DM, Otřísal P, Samphao A. An advanced approach for electrochemical sensing of ibuprofen in pharmaceuticals and human urine samples using a bare boron-doped diamond electrode. J Electroanal Chem. 2018;822:144-52.
4. Kang X, Wang J, Wu H, Liu J, Aksay IA, Lin Y. A graphene-based electrochemical sensor for sensitive detection of paracetamol. Talanta. 2010;81(3):754-9.
5. Palakollu VN, Chiwunze TE, Liu C, Karpoormath R. Electrochemical sensitive determination of acetaminophen in pharmaceutical formulations at iron oxide/graphene composite modified electrode. Arab J Chem. 2020;13:4350-7.
6. Silva FWL, Name LL, Tiba DY, Braz BF, Santelli RE, Canevari TC, et al. High sensitivity, low-cost, and disposability: A novel screen-printed electrode developed for direct electrochemical detection of the antibiotic ceftriaxone. Talanta. 2024;266:125075.
7. Kumar M, Bajpai Tripathy D, Madankar C, Pradhan S. Development and validation of Micellar Liquid Chromatography method for analysis of Paracetamol and Ibuprofen in tablets dosage form. J Indian Chem Soc. 2025;102:101887.
8. Lentini G, Habtemariam S. Microchip capillary electrophoresis–electrospray ionization mass spectrometry analysis of paracetamol metabolites in human urine: An intriguing case. J Chromatogr A. 2014;1327:160.
9. Lourenção BC, Medeiros RA, Rocha-Filho RC, Mazo LH, Fatibello-Filho O. Simultaneous voltammetric determination of paracetamol and caffeine in pharmaceutical formulations using a boron-doped diamond electrode. Talanta. 2009;78:748-52.
10. Švorc L. Determination of caffeine: a comprehensive review on electrochemical methods. Int J Electrochem Sci. 2013;8:5755-73.
11. Koblová P, Sklenářová H, Brabcová I, Solich P. Development and validation of a rapid HPLC method for the determination of ascorbic acid, phenylephrine, paracetamol and caffeine using a monolithic column. Anal Methods. 2012;4:1588.
12. Torres AC, Barsan MM, Brett CMA. Simple electrochemical sensor for caffeine based on carbon and Nafion-modified carbon electrodes. Food Chem. 2014;149:215-20.
13. Zeng Y-L, Huang Y-F, Jiang J-H, Zhang X-B, Tang C-R, Shen G-L, et al. Functionalization of multi-walled carbon nanotubes with poly (amidoamine) dendrimer for mediator-free glucose biosensor. Electrochem commun. 2007;9:185-90.
14. Wu Y, Tang L, Huang L, Han Z, Wang J, Pan H. A low detection limit penicillin biosensor based on single graphene nanosheets preadsorbed with hematein/ionic liquids/penicillinase. Mater Sci Eng C. 2014;39:92-9.
15. Tilahun Yai Feyisa, Shimeles Addisu Kitte DY, Gebretsadik1 and G. Simultaneous Electrochemical Determination of Paracetamol and Caffeine using Activated Glassy Carbon Electrode. Anal Bioanal Electrochem. 2020;12:93-106.
16. Tu NTT, Sy PC, Thien TV, Toan TTT, Phong NH, Long HT, et al. Microwave-assisted synthesis and simultaneous electrochemical determination of dopamine and paracetamol using ZIF-67-modified electrode. J Mater Sci. 2019;54:11654-70.
17. Fernandes DM, Silva N, Pereira C, Moura C, Magalhães JMCS, Bachiller-Baeza B, et al. $MnFe_2O_4$@ CNT-N as novel electrochemical nanosensor for determination of caffeine, acetaminophen and ascorbic acid. Sensors Actuators B Chem. 2015;218:128-36.
18. Latif IA, Merza SH. Fabrication of Functionalize Reduce Graphene Oxide and Its Application in Ampicillin Detection. Nanosci Nanotechnol. 2016;6:24-33.
19. Tchoffo R, Ngassa GBP, Doungmo G, Kamdem AT, Tonlé IK, Ngameni E. Surface functionalization of natural hydroxyapatite by polymerization of β-cyclodextrin: Application as electrode material for the electrochemical detection of Pb (II). Environ Sci Pollut Res. 2022;29:222-35.

pISSN 1859-1388
eISSN 2615-9678

20. BindiyaDey, Manoharan C, Bououdina M, Venkateshwarlu M, Murugan A. Enhanced magnetic, electrochemical and gas sensing properties of cobalt substituted nickel ferrite nanoparticles prepared by hydrothermal route. J Phys Chem Solids. 2023;178:111364.

21. Narang SB, Pubby K. Nickel Spinel Ferrites: A review. J Magn Magn Mater. 2021;519:167163.

22. Ding X, Niu Y, Zhang G, Xu Y, Li J. Electrochemistry in carbon-based quantum dots. Chem Asian J. 2020;15:1214-24.

23. Jihad KM, Roknabadi MR, Mohammadi M, Goharshadi EK. Reduced graphene oxide/TiO_2/$NiFe_2O4$ nanocomposite as a stable photocatalyst and strong antibacterial agent. Sustain Environ Res. 2023; 33.

24. Holzinger M, Goff A Le, Cosnier S. Nanomaterials for biosensing applications: A review. Front Chem. 2014;2:1-10.

25. Wang X, Feng Y, Dong P, Huang J. A Mini Review on Carbon Quantum Dots: Preparation, Properties, and Electrocatalytic Application. Front Chem. 2019;Volume 7 - 2019.

26. Sheshmani S, Mardali M, Shokrollahzadeh S, Bide Y. Starch-derived carbon quantum dots: Unveiling structural insights and photocatalytic potential as a bio-sourced metal-free semiconductor. Int J Biol Macromol. 2024;271:132535.

27. Sudaryanto Y, Hartono SB, Irawaty W, Hindarso H, Ismadji S. High surface area activated carbon prepared from cassava peel by chemical activation. Bioresour Technol. 2006;97:734-9.

28. Tong S-K, Chi P-W, Kung S-H, Wei D-H. Tuning bandgap and surface wettability of $NiFe_2O_4$ driven by phase transition. Sci Rep. 2018;8:1338.

29. Rao R, Zhang X, Sun X, Wang M, Ma Y. Effects of elemental chemical state in $NiFe_2O_4$@ TiO_2 on the photocatalytic performance. J Wuhan Univ Technol Sci Ed. 2020;35:320-6.

30. Bhosale S V, Kanhe NS, Bhoraskar S V, Bhat SK, Bulakhe RN, Shim J-J, et al. Micro-structural analysis of $NiFe_2O_4$ nanoparticles synthesized by thermal plasma route and its suitability for BSA adsorption. J Mater Sci Mater Med. 2015; 26:1–15.

31. Fathy MA, Kamel AH, Hassan SSM. Novel magnetic nickel ferrite nanoparticles modified with poly(aniline- co-o -toluidine) for the removal of hazardous 2,4-dichlorophenol pollutant from aqueous solutions. RSC Adv. 2022;12:7433-45.

32. Taqvi SIH, Solangi AR, Buledi JA, Khand NH, Junejo B, Memon AF, et al. Plant extract-based green fabrication of nickel ferrite ($NiFe_2O_4$) nanoparticles: An operative platform for non-enzymatic determination of pentachlorophenol. Chemosphere. 2022;294:133760.

33. Stachowska JD, Gamża MB, Mellor C, Gibbons EN, Krysmann MJ, Kelarakis A, et al. Carbon Dots/Iron Oxide Nanoparticles with Tuneable Composition and Properties. Nanomaterials. 2022;12:1-18.

34. Liu H, Liang J, Fu S, Li L, Cui J, Gao P, et al. N doped carbon quantum dots modified defect-rich g-C_3N_4 for enhanced photocatalytic combined pollutions degradation and hydrogen evolution. Colloids Surfaces A Physicochem Eng Asp. 2020;591:124552.

35. Minh TT, Phong NH, Van Duc H, Khieu DQ. Microwave synthesis and voltammetric simultaneous determination of paracetamol and caffeine using an MOF-199-based electrode. J Mater Sci. 2018;53:2453-71.

36. Katseli V, Economou A, Kokkinos C. A novel all-3D-printed cell-on-a-chip device as a useful electroanalytical tool: Application to the simultaneous voltammetric determination of caffeine and paracetamol. Talanta. 2020;208:120388.

37. Monteiro MKS, Santos E, Silva DR, Martínez-Huitle CA, Dos Santos E V. Simultaneous determination of paracetamol and caffeine in pharmaceutical formulations and synthetic urine using cork-modified graphite electrodes. J Solid State Electrochem. 2020;24:1789-800.

38. Phong NH, Toan TTT, Tinh MX, Tuyen TN, Mau TX, Khieu DQ. Simultaneous Voltammetric Determination of Ascorbic Acid, Paracetamol, and Caffeine Using Electrochemically Reduced Graphene-Oxide-Modified Electrode. J Nanomater. 2018;2018:1-15.